UC Irvine
UC Irvine Previously Published Works

Title

Measurement of Corneal Elasticity with an Acoustic Radiation Force Elasticity Microscope

Permalink

Journal

ISSN

Authors

Mikula, Eric
Hollman, Kyle
Chai, Dongyul
et al.

Publication Date

2014-07-01

DOI

Peer reviewed

MEASUREMENT OF CORNEAL ELASTICITY WITH AN ACOUSTIC RADIATION FORCE ELASTICITY MICROSCOPE

Eric Mikula[*], **Kyle Hollman**[†,‡], **Dongyul Chai**[§], **James V. Jester**[*,§], and **Tibor Juhasz**[*,§]

[*]Department of Biomedical Engineering, University of California, Irvine, Irvine, California, USA

[†]Department of Biomedical Engineering, University of Michigan, Ann Arbor, Michigan, USA

[‡]Soundsight Research, Livonia, Michigan, USA

[§]Gavin Herbert Eye Institute, University of California, Irvine, Irvine, California, USA

Abstract

To investigate the role of collagen structure in corneal biomechanics, measurement of localized corneal elasticity with minimal destruction to the tissue is necessary. We adopted the recently developed acoustic radiation force elastic microscopy (ARFEM) technique to measure localize biomechanical properties of the human cornea. In ARFEM, a low-frequency, high-intensity acoustic force is used to displace a femtosecond laser-generated microbubble, while high-frequency, low-intensity ultrasound is used to monitor the position of the microbubble within the cornea. Two *ex vivo* human corneas from a single donor were dehydrated to physiologic thickness, embedded in gelatin and then evaluated using the ARFEM technique. In the direction perpendicular to the corneal surface, ARFEM measurements provided elasticity values of $E = 1.39 \pm 0.28$ kPa for the central anterior cornea and $E = 0.71 \pm 0.21$ kPa for the central posterior cornea in pilot studies. The increased value of corneal elasticity in the anterior cornea correlates with the higher density of interweaving lamellae in this region.

Keywords

Cornea; Biomechanics; Elasticity; Elastic modulus; Ultrasound; High-intensity focused ultrasound

INTRODUCTION

Corneal biomechanics plays an important role in determining the shape of the corneal surface and, thus, affects the quality of vision. The air-anterior cornea boundary accounts for nearly two-thirds of the eye's refractive power, and even slight alterations on this surface can cause significant optical aberrations and reduce the quality of vision. Abnormal biomechanical properties have implications in a variety of corneal disorders such as keratoconus, post-LASIK ectasia, astigmatism, myopia and hyperopia.

It has been found that there is significant interweaving of stromal lamellae in the anterior cornea, whereas the posterior cornea has markedly less interweaving (Jester et al. 2010;

Address correspondence to: Eric Mikula, 118 Medical Surge I, Irvine, CA 92697-4375, USA. emikula@uci.edu.

Komai and Ushiki 1991; Radner and Mallinger 2002; Radner et al. 1998). Furthermore, lamellar interweaving markedly increases interlamellar cohesive strength (Smolek 1993; Smolek and McCarey 1990) and protects the anterior region of the cornea against extreme swelling (Muller et al. 2001). This non-uniform structure and varying mechanical behavior suggest an inhomogeneous spatial distribution of corneal elasticity across the corneal thickness. The goal of the study described here was to establish a minimally invasive technique for measurement of corneal elasticity that allows determination of localized corneal elasticity values that can be compared with corneal microstructure at the same location. This would contribute to our understanding of how corneal elasticity and shape are dependent on microstructure and provide insight into biomechanical disorders such keratoconus and corneal astigmatism.

In earlier measurements of corneal elasticity, strip testing and globe inflation methods were used (Hjortdal 1995, 1996; Hoeltzel et al. 1992; Jue and Maurice 1986; Nyquist 1968; Shin et al. 1997; Woo et al. 1972; Zeng et al. 2001). Strip testing involves removing a rectangular-shaped sample from the cornea and then mechanically stretching the strip with increasing force to calculate stress-strain curves. Recently, uniaxial strip testing has been used to evaluate the effect of ultraviolet collagen cross-linking on elasticity (Schumacher et al. 2011). Strip testing was also used to correlate mechanical behavior of the cornea to stromal structure by subjecting corneal strips to uniaxial tension along different directions (Elsheikh and Alhasso 2009). Strip testing lacks the ability to measure the spatial distribution of elastic properties without physically sectioning the cornea into strips from varying regions. Globe inflation assesses elasticity by measuring the displacements of external markers on the corneal surface in response to varying intraocular pressure (IOP). Although globe inflation measures a mean elastic modulus for the entire cornea, or potential elasticity variations across the corneal surface, it clearly lacks the capability to measure the depth dependence of corneal elasticity (Elsheikh et al. 2007; Hjortdal 1996).

Atomic force microscopy has been used to measure the depth dependence of the elastic modulus in the sectioned cornea (Last et al. 2012). In a different study, measurement of the transverse shear modulus at varying depths using torsional rheometry was described (Petsche et al. 2012). However, both of these methods involve physical sectioning of the corneal sample to access the different layers and also have limitations in depth and lateral resolution. The Ocular Response Analyzer (Reichert, Buffalo, NY, USA) measures the deformation of the cornea in response to a brief puff of air and returns corneal hysteresis and corneal resistance instead of elastic modulus (Luce et al. 2005). Corneal hysteresis is a measure of the viscous dampening of the cornea in response to the air puff, and corneal resistance is derived from corneal hysteresis (Bayoumi et al. 2010). Because this method does not require corneal sectioning, it has gained limited use in clinical practice.

Various ultrasonic methods have also been developed for probing the elastic properties of tissues. Shear wave elasticity imaging uses a focused acoustic radiation force to generate shear waves within a tissue. The transverse strain generated by the shear waves is imaged and related to the shear elasticity of the tissue (Sarvazyan et al. 1998). Supersonic shear imaging also uses focused acoustic radiation force to generate shear waves within a tissue, which are imaged and related to elasticity (Bercoff et al. 2004). Supersonic shear imaging

has been used to evaluate the efficacy of photodynamic riboflavin/ultraviolet (UVA)-induced corneal collagen cross-linking (Tanter et al. 2009). Surface wave elastometry measures the speed of acoustic surface waves traveling parallel to the orientation of corneal collagen fibers and relates the propagation velocity to elasticity (Dupps et al. 2007). Similarly, optical coherence tomography has been used to measured shear wave speed in the cornea in response to mechanical perturbation of the corneal surface by a wire (Manapuram et al. 2012). In a variation of this method, an acoustic radiation force was used to perturb the tissue while imaging the tissue vibration with optical coherence tomography (Qi et al. 2012). In acoustic radiation force impulse imaging, high-intensity focused ultrasound pulses are used to directly induce a displacement in the tissue. The displacement of the tissue is tracked using pulse echoes and is related to the mechanical properties of the tissue (Nightingale et al. 2003). In a similar method, corneal strain induced by a metal plate is imaged with an ultrasound elasticity microscope (Hollman et al. 2002, 2013). The ultrasound elasticity imaging techniques described above rely on speckle tracking methods to create the strain images. Elastic properties are calculated from the complex displacement field.

In acoustic radiation force elastic microscopy (ARFEM), a low-frequency, high-intensity acoustic force is used to displace a femtosecond laser-generated microbubble, and high-frequency, low-intensity ultrasound is used to monitor the position of the microbubble within the tissue (Erpelding et al. 2005). The elastic modulus is related to the displacement of the microbubble within the tissue rather than tissue strain. ARFEM has the advantage of improved depth resolution over other ultrasonic methods. Additionally, elasticity is simply related to bubble displacement as opposed to a complex strain image. The location of the elasticity measurement depends solely on the location of the bubble, which can be created anywhere without the need to section the cornea.

To develop a method that can measure the 3-D distribution of elastic properties throughout the cornea, we used ARFEM to measure corneal elasticity in the anterior and posterior central cornea. The ARFEM measurement is similar to the needle indentation method, where a small-area needle is pushed against the corneal surface, and the displacement of the surface is measured to characterize tissue elasticity on the surface (McKee et al. 2011). The clear advantage of ARFEM is that it can measure not only surface location dependence, but also dependence of corneal elasticity on the depth across the entire thickness of the tissue without tissue sectioning. Thus, a 3-D elasticity map of the cornea can be created and compared with local collagen lamellae structure. Because interweaving collagen fibers are especially abundant in the anterior regions of the cornea and their density markedly decreases in the posterior region, the measurement of localized corneal elasticity as a function of depth across the entire thickness of the tissue is important. ARFEM was chosen because it can provide data on the depth dependence of the corneal elasticity obtained with minimally invasive experiments.

METHODS

ARFEM theory

Most ultrasonic radiation force techniques rely on tissue absorption and reflection of ultrasound energy to induce tissue strain and generate strain images, respectively.

Unfortunately, the cornea is neither an efficient absorber nor an efficient reflector of ultrasound. However, the boundary between an aqueous medium, such as the cornea, and a gaseous bubble is nearly a perfect reflector. The reflection coefficient between the aqueous medium and a gaseous bubble is given by

$$R = \left(\frac{Z_2 - Z_1}{Z_2 + Z_1} \right)^2, \quad (1)$$

where R is the reflection coefficient at the boundary, and Z_1 and Z_2 are the acoustic impedances of the two materials (412 and 1.50×10^6 Pa·s/m for air and cornea, respectively). This results in a reflection coefficient of 0.999 for the acoustic wave reaching the bubble within the cornea. For a sound wave traveling in an aqueous medium such as the cornea, nearly 100% of the incoming ultrasound energy incident on a bubble is reflected because of the high acoustic impedance mismatch between aqueous tissue and gas in the bubble. This makes generation of acoustic radiation force twice as efficient as that for a perfect absorber, because the acoustic wave is first stopped and then reversed. In the experiment described in this article, a bubble created in the cornea with a femtosecond laser pulse is pushed by high-intensity focused ultrasound (HIFU) in the direction perpendicular to the corneal surface, referred to as the axial direction, and the axial displacement of the bubble is monitored with a separate low-intensity, high-frequency A-scan ultrasound. The bubble is tens of microns in diameter and vanishes within 1 min.

The elastic modulus of a viscoelastic material can be calculated from the displacement of an embedded microbubble in response to an acoustic radiation force using

$$E = \frac{Ia}{2cx_{\max}} \quad (2)$$

where I is acoustic intensity, a is bubble radius, c is speed of sound in the cornea and $x_{\max}$ is maximum bubble displacement (Ilinskii et al. 2005). The intensity, I, is calibrated before the experiment, whereas bubble radius and maximum displacement are measured experimentally. The speed of sound, c, in water (1500 m/s) was used in all calculations in place of the speed of sound in cornea for convenience. The acoustic intensity is generated by the HIFU element of the transducer in the form of a 2-ms chirped acoustic force pulse. A chirped acoustic force pulse differs from a single-frequency tone burst in that the frequency of the ultrasound wave is swept from 1.4 to 1.7 MHz. This is done to reduce the effect of standing waves in the sample chamber (Erpelding et al. 2007). The intensity of the force pulse was measured using a calibrated needle hydrophone with an active element diameter of 200 μm (Precision Acoustics, Dorchester, Dorset, UK). The central 500 μm of the force beam profile at the focal plane was found to be uniform. Thus, it is reasonable to assume that the bubble, though considerably smaller in diameter than the active element of the hydrophone, was experiencing the same intensity as measured by the hydrophone. The spatial peak, pulse average intensity (I_{sppa}) in the uniform, central area of the focus of the transducer was calculated from the recorded radiofrequency (RF) signal as defined by

$$I_{\text{sppa}} = \frac{\int_{t_1}^{t_2} v^2(t)dt}{10^4 \rho c M_L^2(f_c)\text{PD}}, \quad (3)$$

where v is the signal voltage from the hydrophone (V), ρ is the density of water (kg/m³), c is the speed of sound in water (m/s), M_L is the hydrophone sensitivity (V/Pa) and PD is the force pulse duration (American Institute of Ultrasound in Medicine/National Electrical Manufacturers Association [AIUM/NEMA] 2004). The numerical integral is calculated using the trapezoid method for numeric integration. Bubble radius is measured directly using a light microscope. It was assumed that bubble deformation was negligible during ARFEM measurement because the bubble displacements were less than one and a half times the bubble radius (Ilinskii et al. 2005). With eqns (1) to (3), the elastic modulus of the cornea in the vicinity of a bubble can be calculated by measuring the maximum displacement of the bubble in response to the acoustic radiation force.

ARFEM setup

Figure 1 is a schematic of the ARFEM system. A femtosecond laser is focused into the focal volume of a dual-element, confocal ultrasound transducer. A single laser pulse creates a bubble at a desired location in the cornea. Next, focused ultrasound from the force-generating element pushes on the bubble while the inner tracking element monitors the axial position of the bubble with an A-scan. The sample chamber is mounted to a 3-D micro-stage enabling precise positioning of the bubble within the cornea. The laser and ultrasound foci remain fixed and aligned with each other.

A commercial Ti:sapphire femtosecond laser (Coherent, Santa Clara, CA, USA) is used to create microbubbles in the samples. The laser produces 130-fs pulses at 800-nm wavelength. The beam is focused through a 0.3 NA objective with a working distance of 40 mm. A pulse energy of 80 μJ is used for bubble creation. The ultrasound transducer used to probe the microbubble was custom built to our specifications by the National Institutes of Health Resource Center for Ultrasonic Transducer Technology at the University of Southern California. The transducer consists of two confocal elements. The bubble tracking element (inner) is a 1–3 PZT crystal with a diameter of 15 mm and has a center frequency of 17 MHz with an f-number of 2.9. The HIFU acoustic radiation force-generating element (outer) is a PZT-4 crystal with a 30-mm diameter and has a center frequency of 1.5 MHz with an f-number of 1.4. Both have a focal length of 41 mm. The I_{sppa} of the force-generating element is 125 W/cm².

Figure 2 is a schematic of the wiring for synchronization of inner and outer ultrasound elements, as well as the digitizing board. Synchronization between the force element, imaging element and digitizing board is necessary to ensure that the position of the bubble is measured exactly when the force is turned off. The tracking element is driven by a commercial pulser-receiver (Model 5072 PR, Panametrics, Waltham, MA, USA) at a pulse repetition frequency of 5 kHz, giving one A-scan every 200 μs. The pushing element is

driven by an arbitrary function generator (Model 3314a, Agilent Technologies, Palo Alto, CA, USA) feeding a 50-dB amplifier (ENI Model 240 L, MKS Instruments, Wilmington, MA, USA). The chirped acoustic force pulse waveform is created in MATLAB (The MathWorks, Natick, MA, USA) and exported to the function generator. The waveform consists of a train of 10 force pulses, each 160 μs in duration and swept in frequency from 1.4 to 1.7 MHz, with a 40-μs delay between force pulses (2 ms total). Thus, the strong force pulse, which is a source of noise, is turned off when the reflected tracking pulse reaches the transducer. RF signals from the tracking element are captured by a digitizing board (Agilent Technologies) on a PC sampling at 100 MS/s. All components are synchronized to a 10-MHz master clock. Furthermore, the A-scan tracking pulses are synchronized with an additional tunable delay to ensure that they are triggered during the 40-μs delay between force pulses. This drastically reduces noise in the A-scan and enables tracking of the bubble while it is being displaced. In Figure 3 is the A-scan, HIFU synchronization scheme.

Sample preparation

Two human cadaver eyes from the same donor were obtained from the San Diego Eye Bank. The eyes were preserved within 24 h of death and stored no longer than 5 d. Before the experiment, corneas were thinned to a physiologic thickness of 500–570 μm by inflating the intact globe with 20% Dextran solution at 20 mm Hg IOP. Central corneal thickness was monitored using a Reichert IOPAC pachymeter (Reichert, Depew, NY, USA). The cornea was then excised, leaving a 2-mm scleral rim, and embedded in a 7.5% gelatin gel within the acoustic chamber. To avoid any effect of corneal hydration on the experiments, corneal thickness was also monitored during the ARFEM studies by the echoes of the tracking pulse from the anterior and posterior corneal surfaces. Experiments were performed only when the corneal thickness was in the physiologic range 500 to 570 μm.

Gelatin phantoms

Acoustic radiation force elastic microscopy measurements were conducted in gelatin phantoms and compared against needle indentation measurements in the same phantoms. In this method, a flat-ended cylinder connected to a load cell is used to indent the sample. The elastic modulus is calculated based on the recorded stress-strain relationship and the geometry of the indenting cylinder (McKee et al. 2011). Measurements were made in gels with concentrations of 5%, 7.5% and 10% by weight.

Data acquisition and analysis

The raw 1-D RF data are sectioned and stacked into a 2-D array, where each column represents a single A-scan. The pulser-receiver triggers the A-scan at a 5-kHz pulse repetition frequency, resulting in a 1-D image of the cornea and bubble in every 200 μs. Thus, the resulting M-scan describes the time evolution of the bubble movement in 200-μs steps. A typical M-scan measurement is illustrated in Figure 4. This figure was derived from a porcine eye and is used here solely for visualization of the actual measurement. The porcine cornea is far thicker and softer than the human cornea, allowing for easier distinction of the anterior, posterior and bubble surfaces. The vertical checkered band is the saturated acoustic radiation force pulse as detected by the tracking element. This image was obtained without notched force pulse A-scan synchronization for the purpose of illustrating the force

pulse during the measurement. With the notched synchronization, the saturated acoustic band is not present in the data. The figure indicates the position of the anterior/posterior corneal surfaces and microbubble before, during and after the chirped force pulse. The small inset figure is one sample A-scan taken from the 2-D image. The bubble is displaced in the direction of the acoustic force and returns to its original position once the force pulse is turned off.

In Figure 4 the vertical acoustic radiation force band is masking the position of the bubble while the force pulse is on. A high-pass (10-MHz) filter is applied to the data in post-processing to remove the low-frequency data contained in the vertical band. Additionally, a 1-MHz high-pass hardware filter on the pulser-receiver is used to further reduce the noise caused by the force pulse. The high-pass filtering along with the notched acoustic force pulse waveform described earlier removes nearly all of the acoustic force pulse signal and noise from the A-scan. As result, bubble position can be measured during the force pulse. Figure 5 illustrates the value of using the notched force pulse waveform. Figure 5a illustrates the data pre-processed with only the high-pass filter, and Figure 5b, the high-pass filtered data collected using the notched force pulse waveform approach.

Bubble displacement is calculated from the RF data using a 1-D cross-correlation method between a reference bubble A-scan and the remaining A-scans. The cross-correlation algorithm computes the time lag between subsequent A-scans of the bubble and compares them with the reference A-scan (original bubble position). To account for movement of the cornea as a whole within the gel in response to the acoustic force pulse, the displacement of the corneal surface is subtracted from the displacement of the bubble when calculating the maximum bubble displacement.

RESULTS

Figure 6 compares ARFEM and needle indentation elasticity measurements in gels of varying concentration. ARFEM measured elastic moduli of 0.82 ± 0.09, 1.09 ± 0.04 and 1.59 ± 0.16 kPa in the 5%, 7.5% and 10% gels, respectively. The indentation method measured 1.11 ± 0.03, 2.28 ± 0.08 and 3.45 ± 0.12 kPa for the 5%, 7.5% and 10% gels. Both methods indicate a linear increase in stiffness with concentration.

Figure 7 illustrates the averaged displacement path of 10 bubbles in the axial direction as a function of time in the anterior 100 μm of the central region of the two human cadaver corneas. The mean bubble diameter was measured to be 22 ± 2 μm. The average bubble displacement and elastic modulus in the anterior region of the two corneas were 3.4 ± 0.60 μm and 1.39 ± 0.28 kPa, respectively. The anterior elastic modulus was 1.42 ± 0.30 kPa in eye 1 and 1.36 ± 0.30 kPa in eye 2. For comparison, measurements were also made 150 μm from the posterior surface of the central region in the same corneas. The average bubble displacement and elastic modulus in the posterior region of the two corneas were 6.9 ± 1.7 μm and 0.71 ± 0.21 kPa, respectively. The posterior elastic modulus was 0.70 ± 0.21 kPa in eye 1 and 0.72 ± 0.24 kPa in eye 2.

DISCUSSION

It is interesting to compare elasticity values obtained in this experiment with values generated from other methods. Recently, articles describing measurements with needle indentation techniques on corneal flaps (Winkler et al. 2011) and with atomic force microscopy (Last et al. 2012) have reported elastic moduli ranging from roughly 0.5 kPa to >100 kPa. Winkler et al. reported average corneal elasticity values in the axial direction from roughly 0.75 kPa in the posterior cornea to 1.75 kPa in the anterior region using the needle indentation method. These results are in good agreement with elasticity values obtained with ARFEM. Additionally, both techniques indicate that the stiffness of the anterior cornea is approximately twice of that of the posterior segment. This observation is consistent with the significant increase in interweaving fibrils present in the anterior cornea (Jester et al. 2010; Komai and Ushiki 1991; Radner and Mallinger 2002; Radner et al. 1998).

Acoustic radiation force elastic microscopy and needle indentation data for gelatin phantoms were also similar. Although there are some small discrepancies in the absolute values, both needle indentation and ARFEM reveal the same linear dependence of elasticity on gelatin concentration. The small discrepancies in absolute value may be explained by the fact that needle indentation measurements are performed on the surface of the gel, whereas ARFEM measurements are bulk measurements inside the material.

It is rather difficult to compare ARFEM data with results obtained with other elastometry methods. For example, torsional rheometry (Petsche et al. 2012) measures the transverse shear modulus, which is considerably different than the axial direction measured by ARFEM. Well-established methods such as strip testing and globe inflation measure elasticity along the direction of the corneal lamellae, where tensile strength is high, and are not comparable to ARFEM. Likewise, ultrasonic shear wave imaging and surface wave elastometry measure propagation along the axis parallel to corneal lamellae. However, ARFEM data are in reasonable agreement with results obtained with elastometry methods testing the same axial component of corneal elasticity, such as needle indentation.

One technical challenge with ARFEM measurements is the inconsistent bubble displacements introduced by standing acoustic waves. Standing waves occur when incoming acoustic waves interfere with earlier waves reflected from the chamber bottom. The incoming waves can either constructively or destructively interfere to cause standing positive and negative pressure peaks, respectively. In addition to sweeping the frequency of the force pulse, we used a long-working-distance focusing objective. The long focal length enabled the tissue sample to be mounted far above the optical window at the bottom of the acoustic chamber. Thus, the diverging reflected acoustic waves were too sparse to significantly interfere with incoming waves in the sample plane. These two improvements, along with the notched acoustic force/tracking pulse synchronization, allowed for predictable bubble displacement, as well as clear imaging of the bubble trajectory. The bubble response in the cornea using ARFEM was similar in shape to the response predicted by the classic Voigt model, with relaxation of the displacements following an exponential path (Walker et al. 2000).

Another technical challenge with the ARFEM technique is the measurement of transverse elasticity in the direction of the corneal lamellae parallel to the corneal surface. With the current technique, elasticity can be measured only in the axial direction, orthogonal to the corneal surface. To accommodate measurements in the transverse direction along the corneal lamellae, the transducer would need to be set to a non-orthogonal angle. This will allow measurements of an angled bubble displacement, which can be broken down into components, giving the axial and transverse elastic moduli.

In vivo applications are prevented with the current setup because the laser beam and ultrasound are positioned on opposing sides of the sample. However, redesign and rearrangement of the ultrasound transducer and focusing optics to the same side of the tissue may allow for *in vivo* applications. Because the current setup prevented us from measuring full globes, the effect of physiologic IOP levels on elasticity could not be investigated. However, conclusions are drawn from relative values of elasticity at different locations, which may not be influenced by a lack of IOP.

Although current measurements were performed on cadaver corneas, after the redesign mentioned in the previous paragraph, the ARFEM system has potential for clinical applications if ultrasound and laser intensity values are within tolerable limits. Toward this end, we compared our intensity values with U.S. Food and Drug Administration safety guidelines. Although the femtosecond laser beam intensity used in the experiment is below the 0.5-W safety limit, the spatial peak, pulse average intensity of the ultrasonic push pulse is approximately four times the Food and Drug Administration limit of 28 W/cm^2. We believe that further optimization of the ARFEM technique will result in a substantial decrease in the required push pulse intensity, as well as the applied laser power, allowing for potential clinical applications. For example, in the current experimental setup, a pulse energy of 80 μJ was used to create the microbubble, whereas typically, pulse energies of just a few micro-joules are sufficient to create optical breakdown in the cornea. The increase in the laser energy required may be explained by the fact that the laser was focused through 4 cm of gelatin before entering the cornea. Because the gelatin surface does not have a controlled optical quality, considerable wavefront distortions are introduced into the beam. This may result in increases in the dimensions of the focal spot, hence the need for higher pulse energies to reliably create microbubbles. Therefore, engineering a beam coupling interface with good optical quality will allow a considerable decrease in the applied laser power.

CONCLUSIONS

We have illustrated that ARFEM can measure localized axial elastic modulus in the human cornea without considerably disturbing its mechanical structure. The technique has high lateral and axial resolution that will allow mapping of elasticity throughout the cornea. Additionally, ARFEM may be re-engineered to measure elasticity *in vivo*, allowing potential future clinical applications in the early diagnosis of mechanically compromised corneas, such as those with keratoconus or corneal ectasia after LASIK surgery.

Acknowledgments

References

American Institute of Ultrasound in Medicine/National Electrical Manufacturers Association. (AIUM/ NEMA). Acoustic output measurement standard for diagnostic ultrasound equipment. Revision 3. Laurel, MD: AIUM; 2004. NEMA Standards Publication UD 2-2004

Bayoumi NH, Bessa AS, El Massry AA. Ocular response analyzer and Goldmann applanation tonometry: A comparative study of findings. J Glaucoma. 2010; 19:627–631. [PubMed: 20179628]

Bercoff J, Tanter M, Fink M. Supersonic shear imaging: A new technique for soft tissue elasticity mapping. IEEE Trans Ultrason Ferroelectr Freq Control. 2004; 51:396–409. [PubMed: 15139541]

Dupps W Jr, Netto M, Herekar S, Krueger R. Surface wave elastometry of the cornea in porcine and human donor eyes. J Refract Surg. 2007; 23:66–75. [PubMed: 17269246]

Elsheikh A, Alhasso D. Mechanical anisotropy of porcine cornea and correlation with stromal microstructure. Exp Eye Res. 2009; 88:1084–1091. [PubMed: 19450454]

Elsheikh A, Wang D, Brown M, Rama P, Campanelli M, Pye D. Assessment of corneal biomechanical properties and their variation with age. Curr Eye Res. 2007; 32:11–19. [PubMed: 17364730]

Erpelding T, Hollman K, O'Donnell M. Bubble-based acoustic radiation force elasticity imaging. IEEE Trans Ultrason Ferroelectr Freq Control. 2005; 52:971–979. [PubMed: 16118978]

Erpelding T, Hollman K, O'Donnell M. Bubble-based acoustic radiation force using chirp insonation to reduce standing wave effects. Ultrasound Med Biol. 2007; 33:263–269. [PubMed: 17306697]

Hjortdal J. Extensibility of the normo-hydrated human cornea. Acta Ophthalmol Scand. 1995; 73:12– 17. [PubMed: 7627752]

Hjortdal J. Regional elastic performance of the human cornea. J Biomech. 1996; 29:931–942. [PubMed: 8809623]

Hoeltzel D, Altman P, Buzard K, Choe K. Strip extensiometry for comparison of the mechanical response of bovine, rabbit, and human corneas. J Biomech Eng. 1992; 114:202–215. [PubMed: 1602763]

Hollman K, Emelianov S, Neiss J, Jotyan G, Spooner G, Juhasz T, Kurtz R, O'Donnell M. Strain imaging of corneal tissue with an ultrasound elasticity microscope. Cornea. 2002; 21:68–73. [PubMed: 11805511]

Hollman K, Shtein R, Tripathy S, Kim K. Using an ultrasound elasticity microscope to map three-dimensional strain in a porcine cornea. Ultrasound Med Biol. 2013; 39:1451–1459. [PubMed: 23683407]

Ilinskii Y, Meegan G, Zabolotskaya E, Emelianov S. Gas bubble and solid sphere motion in elastic media in response to acoustic radiation force. J Acoust Soc. 2005; 117(4, Pt 1):2338–2346.

Jester J, Winkler M, Jester B, Nien C, Chai D, Brown D. Evaluating corneal collagen organization using high-resolution nonlinear optical macroscopy. Eye Contact Lens. 2010; 36:260–264. [PubMed: 20724856]

Jue B, Maurice D. The mechanical properties of the rabbit and human cornea. J Biomech. 1986; 19:847–853. [PubMed: 3782167]

Komai Y, Ushiki T. The three-dimensional organization of collagen fibrils in the human cornea and sclera. Invest Ophthalmol Vis Sci. 1991; 32:2244–2258. [PubMed: 2071337]

Last J, Thomasy S, Croasdale C, Russell P, Murphy C. Compliance profile of the human cornea as measured by atomic force microscopy. Micron. 2012; 43:1293–1298. [PubMed: 22421334]

Luce D. Determining in vivo biomechanical properties of the cornea with an ocular response analyzer. J Cataract Refract Surg. 2005; 31:156–162. [PubMed: 15721708]

Manapuram R, Aglyamov S, Monediado F, Mashiatulla M, Li J, Emelianov SY, Larin KV. In vivo estimation of elastic wave parameters using phase-stabilized swept source optical coherence elastography. J Biomed Opt. 2012; 17:100501. [PubMed: 23223976]

McKee CT, Last JA, Russell P, Murphy CJ. Indentation versus tensile measurements of Young's modulus for soft biological tissues. Tissue Eng Part B Rev. 2011; 17:155–164. [PubMed: 21303220]

Muller L, Pels E, Vrensen G. The specific architecture of the anterior stroma accounts for maintenance of corneal curvature. Br J Ophthalmol. 2001; 85:437–443. [PubMed: 11264134]

Nightingale, K., Palmeri, M., Bouchard, R., Trahey, G. Acoustic radiation force impulse imaging: A parametric analysis of factors affecting image quality. Proceedings, 2003 IEEE Symposium on Ultrasonics; Honolulu, Hawaii. 5–8 October 2003; New York: IEEE; 2003. p. 548-553.

Nyquist G. Rheology of the cornea: Experimental techniques and results. Exp Eye Res. 1968; 7:183–188. [PubMed: 5646606]

Petsche S, Chernyak D, Martiz J, Levenston M, Pinsky P. Depth-dependent transverse shear properties of the human corneal stroma. Invest Ophthalmol Vis Sci. 2012; 53:873–880. [PubMed: 22205608]

Qi W, Chen R, Chou L, Liu G, Zhang J, Zhou Q, Chen Z. Phase-resolved acoustic radiation force optical coherence elastography. J Biomed Opt. 2012; 17:110505. [PubMed: 23123971]

Radner W, Mallinger R. Interlacing of collagen lamellae in the mid-stroma of the human cornea. Cornea. 2002; 21:598–601. [PubMed: 12131038]

Radner W, Zehetmayer M, Aufreiter R, Mallinger R. Interlacing and cross-angle distribution of collagen lamellae in the human cornea. Cornea. 1998; 17:537–543. [PubMed: 9756449]

Sarvazyan A, Rudenko O, Swanson S, Fowlkes J, Emelianov S. Shear wave elasticity imaging: a new ultrasonic technology of medical diagnostics. Ultrasound Med Biol. 1998; 24:1419–1435. [PubMed: 10385964]

Schumacher S, Oeftiger L, Mrochen M. Equivalence of biomechanical changes induced by rapid and standard corneal cross-linking, using riboflavin and ultraviolet radiation. Invest Ophthalmol Vis Sci. 2011; 52:9048–9052. [PubMed: 22025568]

Shin T, Vito R, Johnson L, McCarey B. The distribution of strain in the human cornea. J Biomech. 1997; 30:497–503. [PubMed: 9109561]

Smolek M. Interlamellar cohesive strength in the vertical meridian of human eye bank corneas. Invest Ophthalmol Vis Sci. 1993; 34:2962–2969. [PubMed: 8360028]

Smolek M, McCarey B. Interlamellar adhesive strength in human eye bank corneas. Invest Ophthalmol Vis Sci. 1990; 31:1087–1095. [PubMed: 2354912]

Tanter M, Touboul D, Gennisson J, Bercoff J, Fink M. High-resolution quantitative imaging of cornea elasticity using supersonic shear imaging. IEEE Trans Med Imaging. 2009; 28:1881–1893. [PubMed: 19423431]

Walker W, Fernandez F, Negron L. A method of imaging viscoelastic parameters with acoustic radiation force. Phys Med Biol. 2000; 45:1437–1447. [PubMed: 10870702]

Winkler M, Chai D, Kriling S, Nien C, Brown D, Jester B, Juhasz T, Jester J. Nonlinear optical macroscopic assessment of 3-D corneal collagen organization and axial biomechanics. Invest Ophthalmol Vis Sci. 2011; 52:8818–8827. [PubMed: 22003117]

Woo S, Kobayashi A, Schlegel W, Lawrence C. Nonlinear material properties of intact cornea and sclera. Exp Eye Res. 1972; 14:29–39. [PubMed: 5039845]

Zeng Y, Yang J, Huang K, Lee Z, Lee X. A comparison of biomechanical properties between human and porcine cornea. J Biomech. 2001; 34:533–537. [PubMed: 11266678]
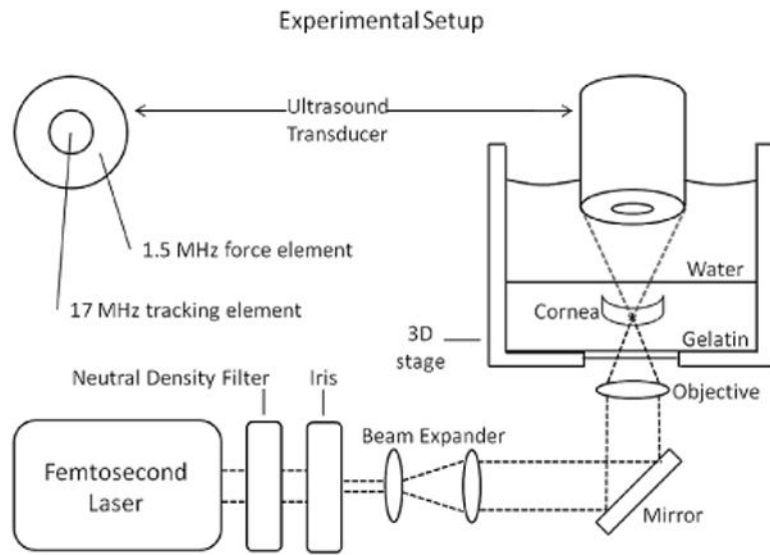
Experimental Setup

Fig. 1.
Experimental setup. The corneal sample and acoustic tank are placed on a 3-D positioning stage that can move independently of the laser and transducer.
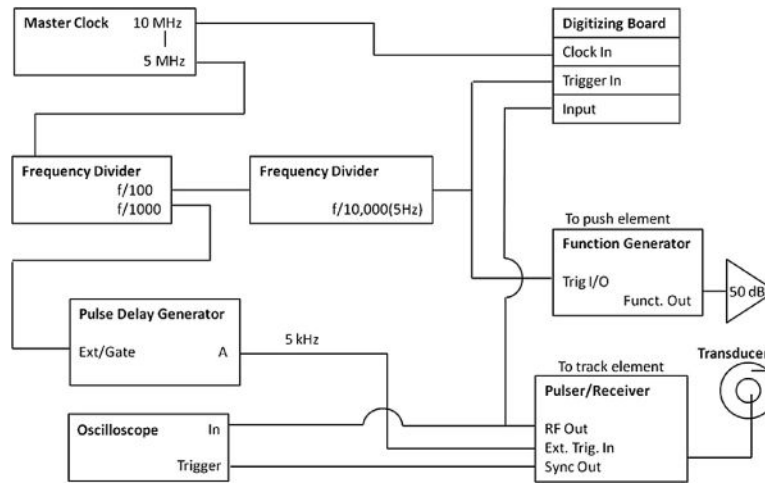
Fig. 2.
Electronic synchronization wiring diagram. All equipment is synchronized to a 10-MHz master clock. The digitizing board samples the radiofrequency (RF) signal at 100 MHz.
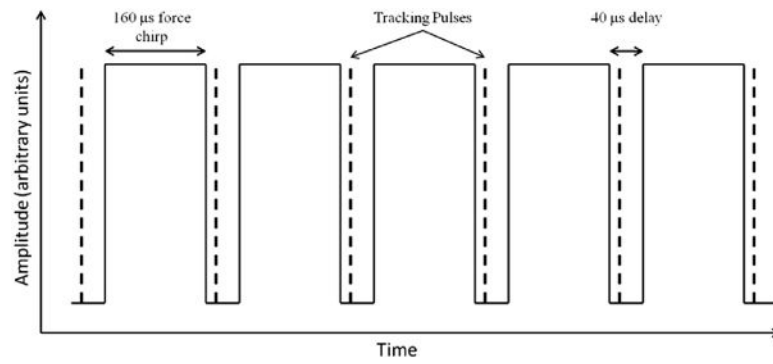
Fig. 3.
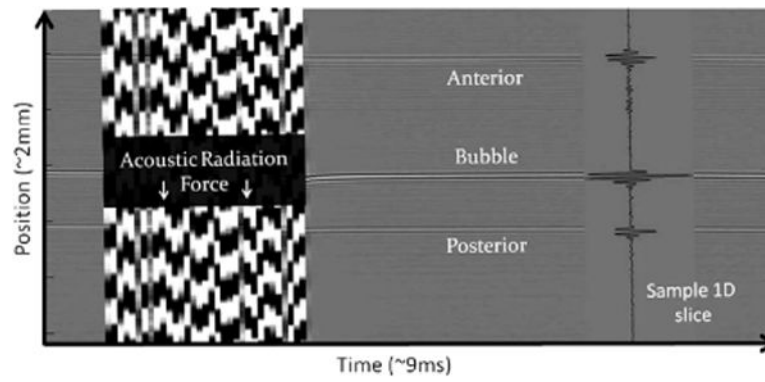Imaging pulses are delayed to coincide with notches between chirped force pulses to remove noise from the A-scans.

Fig. 4.
Sample M-scan from a swollen porcine cornea illustrating the position (y-axis) of the bubble as a function of time (x-axis), as well as the force pulse (vertical band). The y-axis spans about 2 mm, and the x-axis, 9 ms. The sample 1-D slice represents just one of the A-scans at 7-ms time delay taken from the 2-D image.
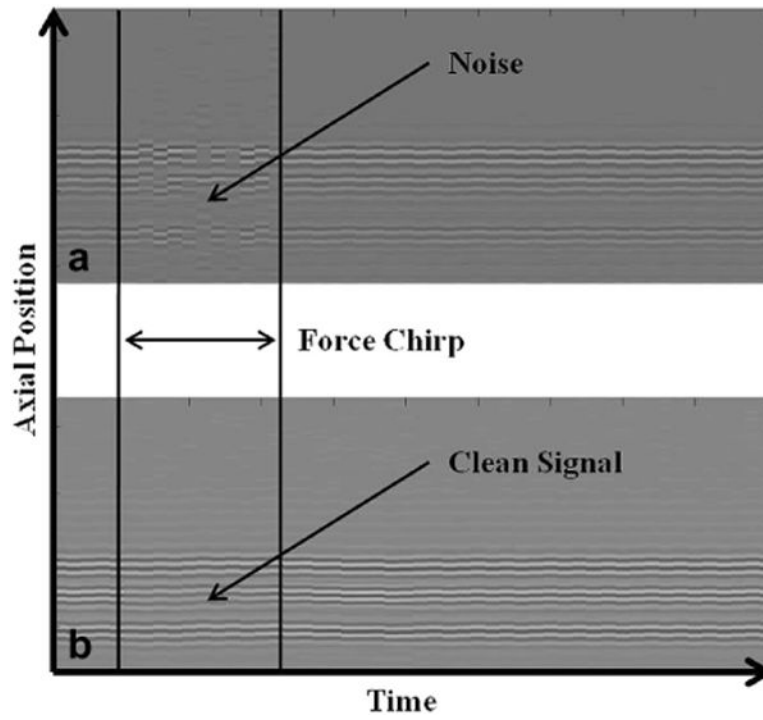
Fig. 5.
(a) Noise leakage from the high-intensity focused ultrasound element into the A-scan, obscuring the position of the bubble during the force chirp. (b) Removal of this noise by synchronization of the A-scan with a notched force pulse.
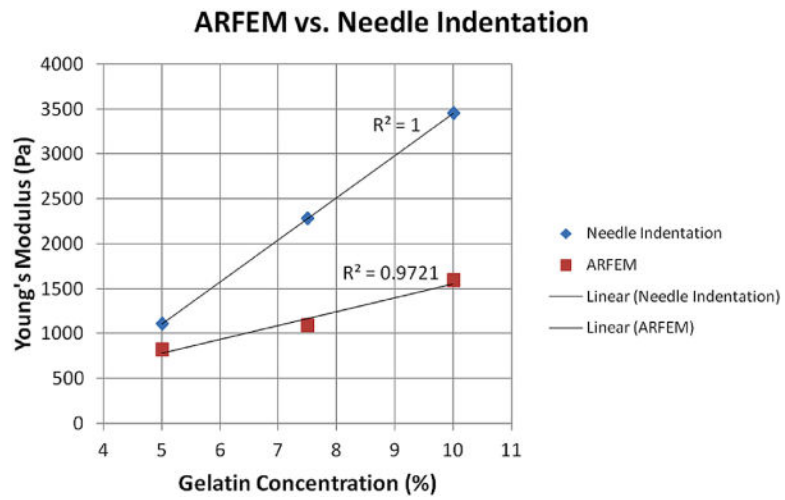
Fig. 6.
Elastic moduli of 5%, 7.5% and 10% gels as measured by acoustic radiation force elastic microscopy (ARFEM) and needle indentation. Solid lines represent linear fits to the data.
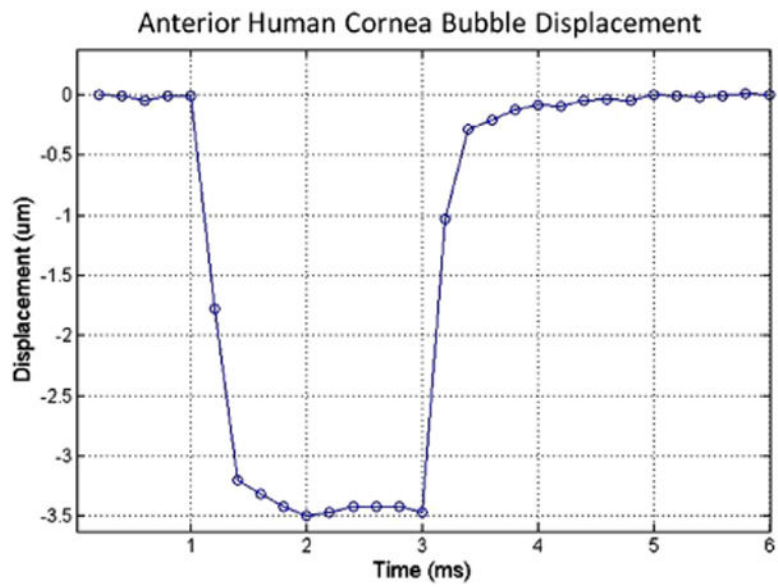
Fig. 7.
Averaged displacement path of 10 bubbles as a function of time in the central anterior of the two human cadaver corneas. The high-intensity focused ultrasound element (HIFU) force is turned on between the 1- and 3-ms marks. The mean displacement was 3.4 ± 0.6 μm, corresponding to an elastic modulus of $E = 1.39 \pm 0.28$ kPa.